KfK 4248
Juli 1987

Density Dependent Effective Interactions and the Determination of Nuclear Densities in Double-Folding Model Analyses of Elastic Alpha-Particle Scattering

H. J. Gils
Institut für Kernphysik

Kernforschungszentrum Karlsruhe

KERNFORSCHUNGSZENTRUM KARLSRUHE

Institut für Kernphysik

KfK 4248

DENSITY DEPENDENT EFFECTIVE INTERACTIONS AND THE DETERMINATION OF NUCLEAR DENSITIES IN DOUBLE-FOLDING MODEL ANALYSES OF ELASTIC ALPHA-PARTICLE SCATTERING

H.J. Gils

Kernforschungszentrum Karlsruhe GmbH, Karlsruhe

Kernforschungszentrum Karlsruhe GmbH
Postfach 3640, 7500 Karlsruhe 1

ISSN 0303-4003

Abstract

Different forms for the density dependence of two-body effective interactions are empirically studied in double-folding model analyses of elastic alpha-particle scattering at E_α = 104 MeV and 140 MeV. The main aspects of the calculations, which are based on the M3Y-interaction, are the analytical parametrisation of the density dependence and the appropriate consideration of the target and projectile density in the overlap region. For the latter purpose different relative weights of the densities were introduced, which also simulate density gradient effects.

Besides the need for a separate treatment of the target and projectile densities in particular the different relative weights are found to be important. With the new modifications suggested in this study consistent results are obtained for the various parametrisations and these results are in agreement with previous implicit folding interpretations of nucleon scattering data.

The results are finally discussed with regard to the ability of getting information about nuclear matter distributions and a comparison with single-folding models is made. It is concluded that double and single-folding models are equivalent when empirical adjustments of parameters are to be made in order to obtain reasonably good fits to the experimental data.

Dichteabhängige effektive Wechselwirkungen und die Bestimmung von Kernmaterieverteilungen in Doppelfaltungsmodell-Analysen der elastischen Alpha-Teilchen-Streuung

Zusammenfassung

Verschiedene Formen der Dichteabhängigkeit effektiver Zwei-Körper-Wechselwirkungen werden in Doppelfaltungsmodell-Analysen der elastischen Alpha-Teilchen-Streuung bei E_α = 104 MeV und 140 MeV empirisch untersucht. Im Vordergrund stehen dabei die analytische Parametrisierung der Dichteabhängigkeit, die geeignete Berücksichtigung der Target- und Projektil-Dichte im Überlappungsbereich und Dichtegradienten-Effekte an der Kernoberfläche. Beim überwiegenden Teil der Rechnungen wird die häufig benutzte M3Y-Wechselwirkung zugrunde gelegt.

Es zeigt sich, daß neben der Notwendigkeit, die Target- und Projektildichte getrennt zu berücksichtigen, vor allem die Gradienten-Effekte eine bedeutende Rolle spielen, die hier erstmals untersucht werden. Mit den in der Arbeit vorgeschlagenen Modifikationen ergeben sich für alle verwendeten Parametrisierungen konsistente Resultate, die auch in guter Übereinstimmung mit impliziten Faltungsmodell-Interpretationen von Nukleon-Streudaten stehen.

Abschließend werden die Ergebnisse im Hinblick auf die Möglichkeit diskutiert, Informationen über nukleare Dichteverteilungen aus der elastischen Alpha-Teilchen-Streuung zu gewinnen. Dazu werden Vergleiche mit früheren Rechnungen im Rahmen des Einzelfaltungsmodells durchgeführt. Es wird gezeigt, daß in beiden Modellen essentielle Parameter empirisch adjustiert werden müssen, um eine angemessene Wiedergabe der Meßdaten zu erhalten. Beide Modelle können daher nur zur Bestimmung von Dichte-*Differenzen* herangezogen werden, wobei die Resultate äquivalent sind.

Contents

1. Introduction

Folding models of the real optical potential using two-body effective interactions provide a realistic microscopic interpretation of nuclear scattering experiments at low and medium energies [1]. The so-called M3Y effective nucleon-nucleon interaction [1,2], for example, was quite successful in describing the elastic and inelastic scattering of heavy ions [1,3]. For the scattering of alpha-particles at energies high enough ($E_\alpha > 80$ MeV) for refractive rainbow scattering to appear at large angles, however, this form of the interaction had to be supplemented by a semi-phenomenological density dependent term [4,5]. Also, in folding model descriptions using other effective interactions was it essential to include density dependence in order to obtain a satisfactory representation of the refraction region of elastic alpha-particle scattering [6-8].

The reason is that refractive alpha-particle scattering probes the nucleus in the whole nuclear surface region and even towards the nuclear interior [6,9-11], where the nuclear density varies from very low values to the value of normal nuclear matter ($\rho \approx 0.17$ fm^{-3}). Most forms of effective interactions, however, were constructed under conditions which correspond to an average over a rather limited range of nuclear densities. In the case of the M3Y-interaction, for example, which is based upon a realistic G-matrix, this average density is about one-third of the density of normal nuclear matter [12].

The origins of the density dependence are mainly Pauli-forbidden intermediate states in the Brueckner reaction matrix [13] and exchange terms. These were studied in extensive work starting from first principles [13,14], and the effects are well understood in direct application to alpha-particle scattering data [7,8,15], too. However, it is very laborious to take such effects into account explicitly in numerous analyses of scattering cross sections e.g. for large series of target isotopes [11,16] or projectile energies [12] where isotopic or energy dependent effects of the optical potential are to be studied . Therefore, in such analyses the density dependence of the two-body effective interaction is usually treated in a semi-phenomenological way using various parametrisations [4-8].

Recently [17], a new form of density dependence due to relativistic virtual-pair effects [18] and three-body force effects [19] was discussed which is in particular important for densities higher than that of normal nuclear matter. Parameters for this form of density dependence were derived [17] in an implicit folding interpretation of elastic nucleon scattering cross sections by various nuclei at

energies between 10 and 65 MeV. A direct application of this form of density dependence in folding model fits to experimental data, however, has not yet been made. It is *one* aim of this paper to compare these various forms of density dependence including this recent form in folding model analyses of extensive and accurate alpha-particle scattering data.

An important question, which generally appears in density dependent *double*-folding calculations of composite projectile scattering, is the way how to take the dependence of the effective interaction on the *projectile* and *target* densities appropriately into account. In many cases [1,4,12,16] the so-called "sudden" or "frozen density" approximation was chosen, where the sum of the projectile and the target densities at the coordinate halfway between the interacting nuclei was used, although this violates actually the Pauli-principle [8]. This is avoided in other approaches [5,7,8] e.g. by introducing separate terms for the projectile and target densities.

In the present study the separated form is modified in a way which allows to introduce the projectile and the target density with different relative weights in the density dependent terms. Such a modification, which was already discussed previously [20], may in particular be important for alpha-particle scattering, since here, in contrast to the scattering of heavy ions, the projectile has a significantly higher density than any medium weight or heavy target nucleus. Therefore, the study of effects of a different weight of projectile and target densities is the *other* aim of this work.

The results of these studies are finally discussed with regard to the possibility of determining nuclear density distributions in *double*-folding model analyses of elastic alpha-particle scattering and a detailed comparison is made with previous *single*-folding model analyses.

Folding model descriptions of the real optical potential are usually justified by comparing the calculated elastic scattering cross sections with experimental data, where the goodness of the fit represented by the value of χ^2 per degree of freedom (χ^2/F) is the relevant criterion. This number plays a corresponding role also in the present studies. In addition, we use another well-defined criterion for the justification of the folded optical potentials which is given by the comparison with so-called "model independent" potential forms [6,9,11,21]. With these potentials the best representation possible of experimental scattering data in terms of a local complex optical potential is achieved [9,11,22,23] and hence these potentials may be regarded as the "true" projectile-target interaction. In analyses

of scattering experiments using "model independent" potentials realistic errors for the potential and its various integral quantities are obtained which provide the well-defined additional criteria for the justification of the folded potentials mentioned above.

It should be emphasized, that the present semi-phenomenological studies of the density dependence of effective interactions are especially relevant for high quality experimental data which are able to reveal small details of the optical potential. Such data from a series of isotopes are available at an energy E_α = 104 MeV [9,11]. Experimental data at E_α = 140 MeV [24,25] were also analysed.

2. Methods

In the double-folding model for composite projectile elastic scattering the real part of the central optical potential is written as

$$Re\,U(\mathbf{r}) = \lambda_R \int\int V_{NN}(\mathbf{r}_{NN},\rho)\ \rho_T(\mathbf{r}_T)\ \rho_P(\mathbf{r}_P)\ d^3r_T\ d^3r_P \qquad (1)$$

where ρ_P and ρ_T are the nuclear matter densities of the projectile and target, respectively, V_{NN} is the density dependent effective nucleon-nucleon (NN) interaction, and λ_R is a phenomenological normalisation factor. The coordinates are explained in Fig. 1. In most applications of this model it was assumed that V_{NN} could be factorised [26] into a density independent radial part $t(r_{NN})$ and a density dependent term $g(\rho)$

$$V_{NN}(\mathbf{r}_{NN},\rho) = t(\mathbf{r}_{NN})\cdot g(\rho) \qquad (2)$$

For the radial part of the effective interaction we use the M3Y-form [1,2] which is given by

$$\begin{aligned} t^{M3Y}(\mathbf{r}_{NN}) = \quad & V_1 \exp(-a_1 r_{NN})/(a_1 r_{NN}) \\ & + V_2 \exp(-a_2 r_{NN})/(a_2 r_{NN}) \\ & + \hat{J}_{00}\,\delta(\mathbf{r}_{NN}) \end{aligned} \qquad (3)$$

where the zero-range term $\hat{J}_{00}\ \delta(r_{NN})$ is energy dependent and considers approximately exchange effects [1]. The parameter values are

V_1 = 7999 MeV
a_1 = 4.0 fm^{-1}
V_2 = -2134 MeV
a_2 = 2.5 fm^{-1}

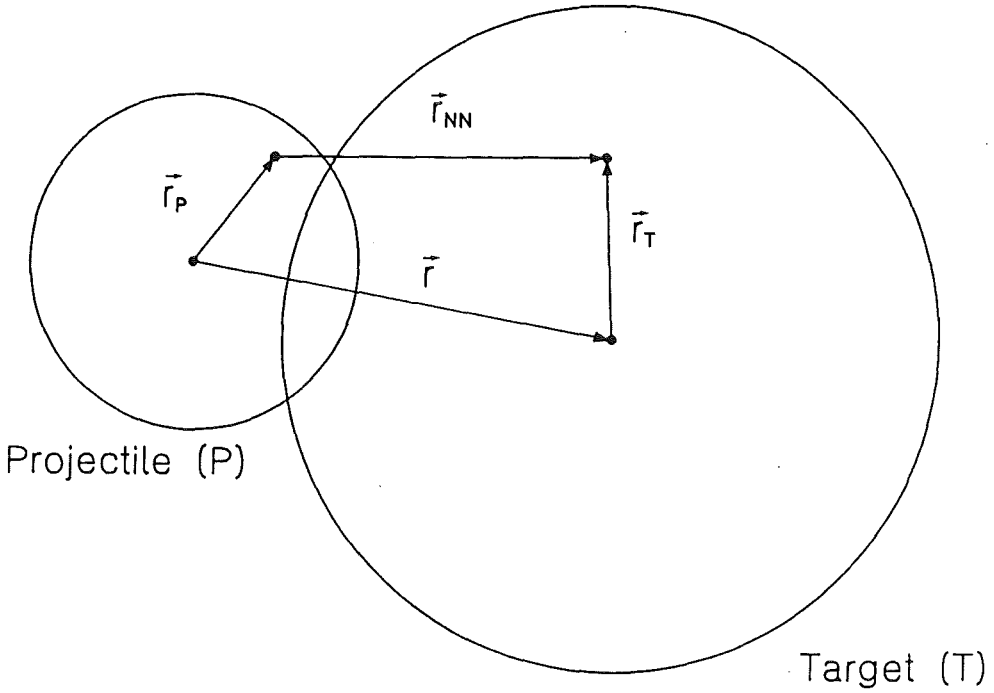

Fig. 1 Coordinates used in the projectile-target system

Table 1: Parameter values of the density dependent M3Y effective interaction [12].

E_a (MeV)	c_ρ	a	β (fm^3)
104	0.3496	4.38	8.422
140	0.279	5.141	7.202

The strength of the exchange term is [4,12]

$\hat{J}_{00} = -240.1$ MeV fm^3 for $E_\alpha = 104$ MeV
$\hat{J}_{00} = -227.7$ MeV fm^3 for $E_\alpha = 140$ MeV

In the so-called density dependent M3Y-interaction the term g(ρ) is written as [4]

$$g(\rho) = c_\rho \{1 + \alpha \exp[-\beta(\rho_T(\mathbf{r}_T) + \rho_P(\mathbf{r}_P))]\} \qquad (4)$$

This form is adopted unaltered as one possible parametrisation and is denoted as DD M3Y. The corresponding parameter values of c_ρ, α and ß are given in Table 1.

Another widely used form for the density dependence is [6,13,27]

$$1 - \gamma \rho^{2/3},$$

and more recently [17] the form

$$1 - \gamma \rho^3$$

was suggested, where γ is an empirical parameter. As already done by Chaudhuri [5] for the former case we introduce a projectile-density and target-density dependent factor of these forms, namely

$$g(\rho) = \left| 1 - \gamma \rho_T^{\frac{2}{3}}(\mathbf{r}_T) \right| \left| 1 - \gamma \rho_P^{\frac{2}{3}}(\mathbf{r}_P) \right| \qquad (5)$$

and correspondingly for the case of the cubic density dependence.

As a new modification these terms are supplemented with the possibility of having a different weight which can be changed easily and a clear-cut way . The relative weights of the projectile and target-density terms are given by additional weight factors w and (1-w), respectively, multiplying the density dependence parameter γ, with $0 \le w \le 1$.Hence, we have

*DD*2/3:
$$g(\rho) = \left| 1 - w\,\gamma \rho_T^{\frac{2}{3}}(\mathbf{r}_T) \right| \left| 1 - (1-w)\gamma \rho_P^{\frac{2}{3}}(\mathbf{r}_P) \right| \qquad (6)$$

or

*DD*3:
$$g(\rho) = \left| 1 - w\,\gamma \rho_T^{3}(\mathbf{r}_T) \right| \left| 1 - (1-w)\gamma \rho_P^{3}(\mathbf{r}_P) \right| \qquad (7)$$

It should be noted that such different weights also simulate density *gradient* effects in the local-density approximation (LDA) [20] of the projectile-target

overlap region due to the different coordinates r_T and r_P occurring in the two factors. These gradient effects can be expected to be important at the potential surface. This can be concluded from similar single-folding model studies [20] where an approximation for the density dependence in formal analogy to eq. (6) was quite successful. In this simpler case the parameter w was *only* representative for gradient effects of the target density, since the corresponding term g(ρ) varied with varying w only if $\rho_T(r_T) \neq \rho_T(r_P)$. In the present case of double-folding the gradient effects cannot be separated from other effects such as different density compression since all these effects are phenomenologically accounted for by the parameter w.

The modification of separated projectile and target-density terms can also be introduced in the DD M3Y-interaction writing

$$\text{DDexp}: \qquad g(\rho) = c_\rho \{1 + \alpha \exp[-\beta'(w\rho_T(r_T) + (1-w)\rho_p(r_p))]\} \qquad (8)$$

With ß' = 2 ß and w = 0.5 this corresponds to the usual DD M3Y-interaction (eq. 4).

An apparently important point in folding model analyses is the treatment of the *imaginary* part of the optical potential. Several forms such as the standard Woods-Saxon (WS) or the squared Woods-Saxon form (WS^2) with and without surface term were used in the past [4,7,11,15] and it was, sometimes, concluded that the latter form (WS^2) with surface term should be preferred. This will briefly be discussed here .

For alpha-particle scattering in the energy range treated in this study it is well known that deficiencies in the form of the *real* potential can partly be compensated by variation of the imaginary potential in order to get a better fit to experimental data and vice versa. This behaviour often led to confusion about the most suitable form for the imaginary potential [4]. A clear answer to this question was given by phenomenological studies using "model independent" potential forms such as the Fourier-Bessel (FB) potential [21]. It was shown [23] that once the *real* part of the optical potential has the best "model independent" form WS and WS^2 imaginary potentials are equivalent and even the use of a model independent imaginary potential does not further improve the fit to the scattering data.

The reason for this observation is that the imaginary potential is well determined only in a limited radial region which can sufficiently well be approximated by either of the mentioned model forms [23]. Therefore, standard WS

imaginary potentials were used in the present studies the parameters of which were fitted to the scattering cross sections. Deviations of these parameters or of radial moments of the imaginary potentials from the values found together with a "model independent" real potential are, besides others, an indication for deficiencies in the folded *real* potential.

3. Analyses and results

The different models for the density dependence of the effective NN-interaction were studied using the elastic alpha-particle scattering data for ^{40}Ca, ^{50}Ti, ^{52}Cr at E_α = 104 MeV [9,11] and for ^{40}Ca and ^{50}Ti at E_α = 140 MeV [24,25]. These data were selected, because many other optical model studies with different aims were previously performed [4-12,15,20-25,28] with the same data or parts of it so that wide and general comparisons are possible. Also, each of these angular distributions was previously analysed, in a consistent manner, in the framework of the "model independent" Fourier-Bessel potential [10,11,21] providing the measure for the justification of the present studies. The results of the FB-analyses, taken from Refs. 10,11 and 29, are shown in Table 2 for comparison with the present analyses.

Since ^{40}Ca is often used as "benchmark" nucleus in studies of isotopic series and since its nuclear matter distribution is assumed to be reliably known, most of the studies were done for this nucleus, especially also because these are the most accurate experimental data [28].

The target nuclear matter density distributions needed for the analyses were adopted from shell-model calculations of Brown et al. [30] (^{40}Ca) and from Hartree-Fock calculations [31] (^{50}Ti, ^{52}Cr). These densities are in agreement with experimental charge distributions. In some calculations (Sect. 3.5.) phenomenological two-parameter Fermi functions (F2) and "model independent" Fourier-Bessel (FB) forms were used for the target densities. For computational convenience the density of the projectile was assumed to have a Gaussian form with the same size parameter a^2 = 0.7024 fm^{-2} as used in many other work [1,5,7,15,16].

Table 2: Integral moments of the real (v) and imaginary (w) alpha-particle scattering optical potentials from "model independent" analyses and values of χ^2/F obtained in the fits [10,11,29].

E_α (MeV)	Target	$-J_v/4A$ (MeV fm^3)	$\langle r_v^2\rangle^{1/2}$ (fm)	$-J_w/4A$ (MeV fm^3)	$\langle r_w^2\rangle^{1/2}$ (fm)	χ^2/F
104	^{40}Ca	324.8 ± 3.0	4.345 ± 0.022	103.0	4.934	2.2
	^{50}Ti	304.0 ± 3.6	4.446 ± 0.023	93.2	5.048	1.6
	^{52}Cr	300.4 ± 3.8	4.460 ± 0.024	96.2	5.088	1.5
140	^{40}Ca	322.4 ± 3.4	4.414 ± 0.033	107.	4.878	0.8
	^{50}Ti	305.9 ± 3.4	4.573 ± 0.044	96.	5.102	2.0

3.1. CONVENTIONAL DENSITY DEPENDENT DOUBLE-FOLDING

The experimental data were first analysed using the density dependent M3Y-interaction (DD M3Y) as introduced by Kobos *et al.* [4] varying only the normalisation parameter λ_R together with the imaginary potential. As an example, the experimental and calculated cross sections for ^{40}Ca at $E_\alpha = 104$ MeV are displayed in Fig. 2 (upper part). The results compiled in Table 3 are consistent with the previous ones [4] where slightly different target density distributions might have been used. When comparing the results with those from Table 2 it is obvious that the folded potentials have too small volume integrals and root-mean square (rms) radii and are, in most cases, too deep in the nuclear interior, as shown in Fig. 3.

3.2. SEPARATE TARGET AND PROJECTILE DENSITY DEPENDENCE

In the next step of the analyses the density dependence was factorised into a target and a projectile density term with equal weights ($w = 0.5$) and the three different parametrisations as introduced in Sect. 2 (eq. 6-8) were used. The zero-range exchange pseudo-potential was included as before. The parameters β' or γ were adjusted in the fits to the data together with λ_R and the imaginary potential. The results for ^{40}Ca at $E_\alpha = 104$ MeV are shown in Table 4a.

Looking first at the exponential density dependence (DDexp) it is interesting to note that the normalisation parameter λ_R is now unity within the error. Moreover, the parameter β' is considerably smaller than $2\beta = 16.822$ fm^3 (see Table 1) which may be interpreted as meaning that there is no full density compression ("frozen density approximation") in the overlap region of target and projectile. In other words, the violation of the Pauli-principle [8] is automatically removed with this modification of the DD M3Y-interaction [4] and no renormalisation of the potential is necessary ($\lambda_R = 1$).

The resulting parameter values for the other two parametrisations DD2/3 and DD3 can be compared with previous work, where $\gamma = 1.5 \pm 0.2$ fm^2 [17] and $\gamma \approx 1.9$ fm^2 [32] was derived for the $\rho^{2/3}$ dependence and $\gamma = 67 \pm 12$ fm^9 [17] for the cubic density dependence in implicit folding interpretations of various scattering experiments. These values seem to deviate from those obtained in the present direct double-folding analyses. However, the implicit folding interpretation is based on the assumption $\lambda_R = 1$. Since there is a strong correlation

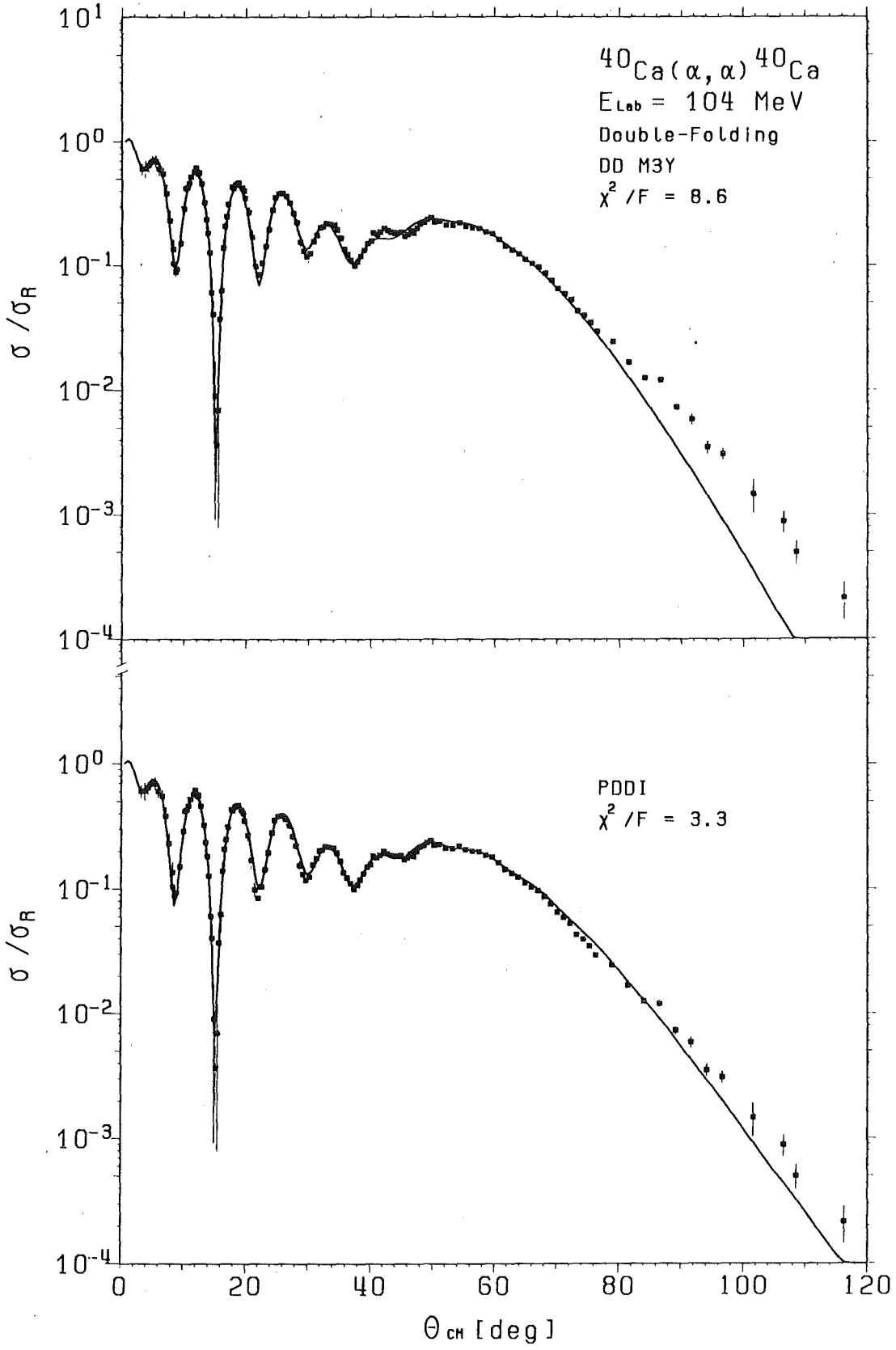

Fig. 2 Experimental and calculated differential cross sections for elastic alpha-particle scattering by ^{40}Ca at E_α = 104 MeV
Upper part: DD M3Y-interaction [4]
Lower part: Phenomenological interaction (see Sect. 3.4.)

Table 3: Normalisation factor λ_R and integral moments of the double-folding optical potentials using the DD M3Y-interaction [4] (see text). Also shown are the rms radii $<r_m^2>^{1/2}$ of the calculated nuclear matter densities [30,31] used for the analyses. Numbers in brackets are the errors (last digits).

E_α (MeV)	Target	$<r_m^2>^{1/2}$ (fm)	λ_R	$-J_v/4A$ (MeV fm^3)	$<r_v^2>^{1/2}$ (fm)	$-J_w/4A$ (MeV fm^3)	$<r_w^2>^{1/2}$ (fm)	χ^2/F
104	^{40}Ca	3.369	1.262(3)	308.8	4.266	98.4	5.081	8.55
	^{50}Ti	3.542	1.239(3)	295.8	4.403	89.7	5.123	3.92
	^{52}Cr	3.576	1.239(4)	294.5	4.431	94.9	5.225	6.57
140	^{40}Ca	3.369	1.309(10)	294.6	4.283	94.8	4.970	11.10
	^{50}Ti	3.542	1.290(6)	283.3	4.421	89.3	5.183	9.61

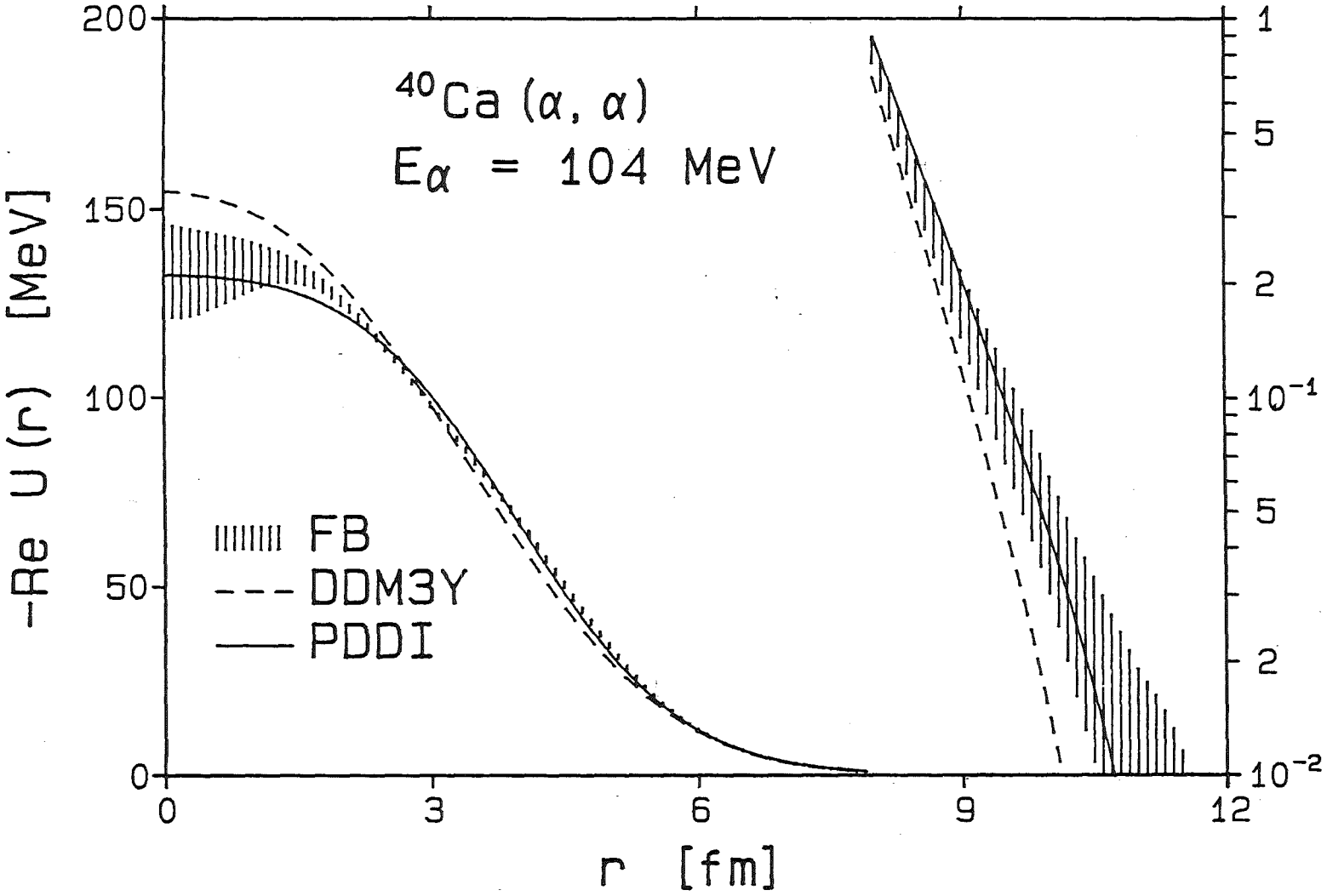

Fig. 3 Real optical potential for elastic alpha-particle scattering by ^{40}Ca at E_α = 104 MeV from different analyses
Hatched: FB-potential [11]
Dashed: DD M3Y-interaction
Solid: Phenomenological interaction (see Sect. 3.4.)

Table 4a: Optical potentials for $^{40}Ca(\alpha,\alpha)$ at E_α = 104 MeV obtained from double-folding model fits using the M3Y effective interaction and separate target and projectile density terms with equal weights (w = 0.5, see text). Number in brackets are the errors (last digits).

Model	λ_R	β' (fm^3)	Y	$-J_v/4A$ (MeV fm^3)	$\langle r_v^2\rangle^{1/2}$ (fm)	$-J_w/4A$ (MeV fm^3)	$\langle r_w^2\rangle^{1/2}$ (fm)	χ^2/F
DD exp	0.997(32)	11.66(57)	-	303.4	4.234	97.9	5.009	6.76
DD2/3	1.829(38)	-	2.887(49)*	304.8	4.235	98.4	5.005	6.44
DD3	1.386(24)	-	82.9(1.5)**	300.3	4.208	98.5	5.029	8.59

Table 4b: Same as Table 4a, but different weights (w = 0.8, see text)

Model	λ_R	β' (fm^3)	Y	$-J_v/4A$ (MeV fm^3)	$\langle r_v^2\rangle^{1/2}$ (fm)	$-J_w/4A$ (MeV fm^3)	$\langle r_w^2\rangle^{1/2}$ (fm)	χ^2/F
DD exp	0.783(14)	7.99(24)	-	307.0	4.242	99.5	4.981	5.41
DD2/3	1.478(21)	-	2.267(32)*	308.9	4.249	99.7	4.974	5.12
DD3	1.288(16)	-	123.6(2.2)**	308.5	4.244	100.7	4.950	5.58

*fm^2 **fm^9

between λ_R and γ [20] (see Fig. 4) a scaling of the latter parameter has to be made. This leads to $\gamma \approx 1.3$ fm^2 for the $\rho^{2/3}$-dependence and $\gamma \approx 70$ fm^9 for the cubic density dependence which is in agreement with other analyses [17,32].

When comparing the results for the $\rho^{2/3}$ -dependence (DD2/3) with the studies of Chaudhuri [5], who first applied this model to part of the same alpha-particle scattering data used here, a considerable discrepancy of the derived parameter values λ_R and γ is observed. This is due to the fact that this author used unrealistic nuclear densities (two-parameter Fermi form) the rms-radii of which were about 0.1 fm larger than the experimental values [11,33], namely $<r_m^2>^{1/2}$ = 3.446 fm (^{40}Ca), $<r_m^2>^{1/2}$ = 3.648 fm (^{50}Ti) and $<r_m^2>^{1/2}$ = 3.686 fm (^{52}Cr).

The density dependent factors $\lambda_R \cdot g(\rho)$ of the various forms are shown in Fig. 5 (upper part). The three curves meet closely at a density of about $\rho = 0.025$ fm^{-3} which corresponds to a target nuclear radius of about r = 4.6 fm and a potential radius of about r = 6.5 fm. This radial region of the potential is known [11,23] to be well determined by the diffraction part of the experimental data used.

3.3. DIFFERENT WEIGHTS FOR THE TARGET AND PROJECTILE-TERM

We study now the influence of different weights for the target and projectile density terms on the parameters and on characteristic quantities of the optical potentials and on the representation of the experimental data. For that purpose the weight parameter w is varied between w = 0, where the dependence on the target density is neglected, and w = 1, where the dependence on the projectile density is neglected. It is emphasized, again, that this modification also simulates *gradient* effects in the folded potentials [20].

The results of the analyses for ^{40}Ca at E_α = 104 MeV are shown in Fig. 6 for the three parametrisations. It is obvious that in all cases a better representation of the experimental data is obtained for w > 0.5 and the value w = 0.8 may be representative as average best value for all cases. The characteristic quantities of the optical potentials for w = 0.8 are compiled in Table 4b. It is interesting to note that in this case the three parametrisations are fully equivalent in fitting the data. Also, the values of the parameters are better determined than for w = 0.5.

The density dependence factors $\lambda_R \cdot g(\rho)$ are displayed in the lower part of Fig. 5. These curves are much closer over a wide range of densities than for w = 0.5 and in addition to the crossing point around $\rho = 0.02$ fm^{-3} another

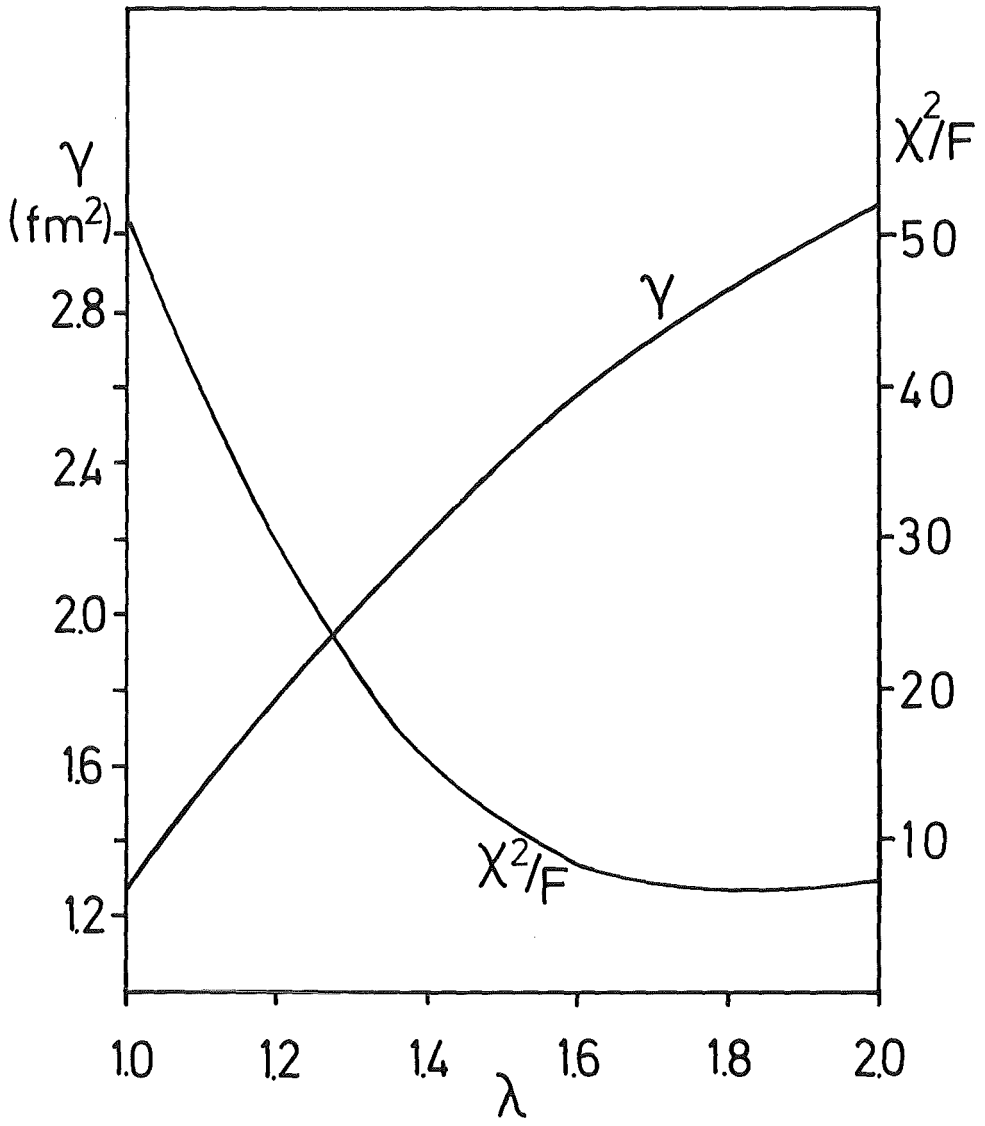

Fig. 4 Correlation between the parameters λ_R and γ and corresponding values of χ^2/F for the $\rho^{2/3}$ density dependence

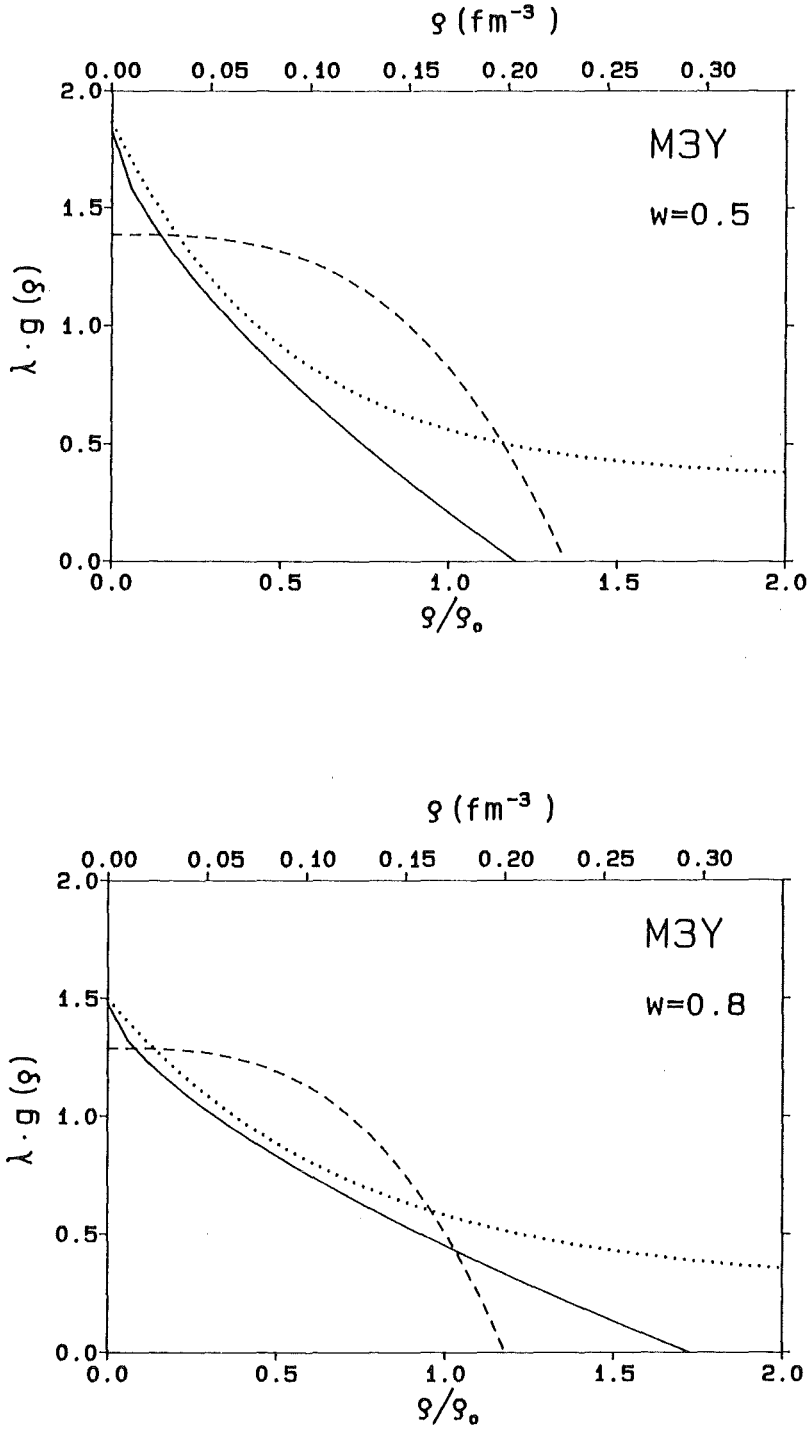

Fig. 5 Density dependence of the M3Y-interaction (see text)
Solid: DD 2/3
Dashed: DD3
Dotted: DD$_{exp}$

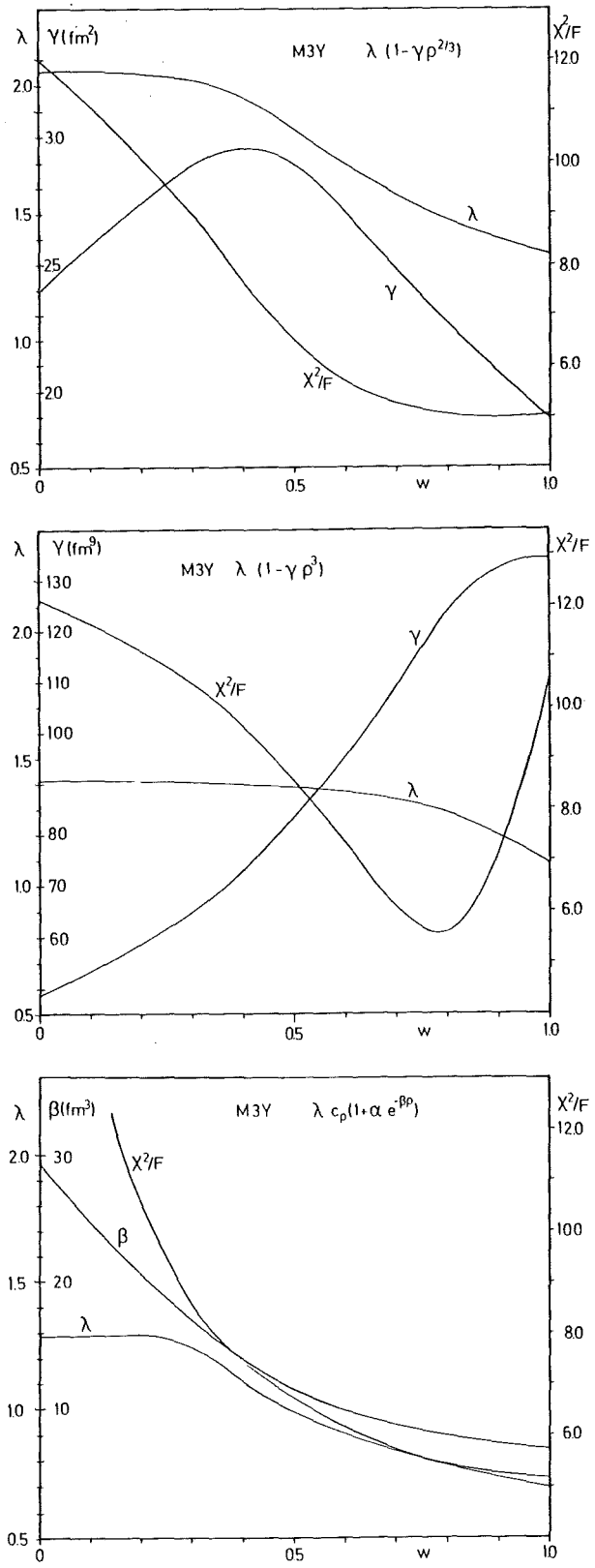

Fig. 6 Dependence of parameters λ_R, β' and γ on the weights of the density dependent terms and corresponding values of χ^2/F

crossing point appears around $\rho = 0.17$ fm^{-3} corresponding to a target nuclear matter radius of $r \lesssim 1.5$ fm and a potential radius of $r \lesssim 3$ fm. The real optical potential at this radius is well determined by the refraction region of the experimental data [11,23].

In Table 5 it is shown that the modification of separate target and projectile density terms with different weights leads to a clear improvement of the fits also for the other target nuclei and energies studied. The same is observed for the other parametrisations not included in Table 5. Similarly good fits are obtained using fixed average values for $\gamma = 2.267$ fm^2 (104 MeV) and $\gamma = 2.528$ fm^2 (140 MeV)and varying only λ_R.

Since the way in which a variable weight of the target and projectile density was introduced in these studies was purely phenomenological a physical interpretation of the above findings is not easy and cannot easily be proved. However, one should keep in mind the origins of the density dependence which are closely related to the nuclear structure. Since the structure of the alpha-particle is considerably different from the average structure of heavier nuclei, such a different weight in density dependent effective interactions is more probable than an equal weight.

The average best value $w \approx 0.8$ found in the analyses for the relative weight may be interpreted as meaning that the strength of the free NN-interaction is reduced in the nuclear medium of the overlap region mainly due to the *target* nuclear matter density rather than the projectile density. This seems a plausible consequence of the different nuclear structure. Interpretations in terms of effective densities (DD2/3, DD3) or different density compressions lead also to the reasonable result that the projectile is more inert than the target.

The importance of density gradient effects for the present results cannot as easily be stated as in previous single-folding model studies [20]. When comparing in detail the potential forms obtained in the analyses one recognizes that the variation of the parameter w mainly influences the potential surface whereas the flat region in the interior shows little dependence. However, the various possible contributing effects cannot be disentangled in this simple empirical picture. For that purpose detailed studies on a more fundamental basis may be useful.

Table 5a: Parameters and integral moments of the optical potentials using the M3Y-interaction [1,2] and the $\rho^{2/3}$-density dependence with different weights (w = 0.8) for the target and projectile density (see text).

Energy (MeV)	Target	λ_R	Y (fm^2)	$-J_v/4A$ (MeV fm^3)	$\langle r_v^2\rangle^{1/2}$ (fm)	$-J_w/4A$ (MeV fm^3)	$\langle r_w^2\rangle^{1/2}$ (fm)	χ^2/F
104	^{40}Ca	1.478(21)	2.267(32)	308.9	4.249	99.7	4.974	5.12
	^{50}Ti	1.512(13)	2.345(20)	298.3	4.403	92.7	5.072	2.01
	^{52}Cr	1.334(19)	2.030(32)	293.1	4.384	96.8	5.109	2.80
140	^{40}Ca	1.629(31)	2.528(39)	300.8	4.303	100.5	4.922	5.55
	^{50}Ti	1.641(22)	2.552(26)	289.8	4.449	94.8	5.134	4.72

Table 5b: Same as 5a, but with the parameter $\gamma = 2.267$ fm^2 ($E_\alpha = 104$ MeV) and $\gamma = 2.528$ fm^2 ($E_\alpha = 140$ MeV) fixed

E_α (MeV)	Target	λ_R	$-J_v/4A$ (MeV fm^3)	$\langle r_v^2 \rangle^{1/2}$ (fm)	$-J_w/4A$ (MeV fm^3)	$\langle r_w^2 \rangle^{1/2}$ (fm)	χ^{2}/F
104	^{40}Ca	1.477(3)	308.7	4.249	99.8	4.974	5.03
	^{50}Ti	1.461(3)	296.8	4.390	92.3	5.057	2.15
	^{52}Cr	1.470(4)	297.0	4.419	98.1	5.157	3.67
140	^{40}Ca	1.628(9)	300.6	4.303	100.3	4.920	5.43
	^{50}Ti	1.621(8)	289.0	4.445	95.4	5.126	4.77

3.4. RADIAL PART OF THE EFFECTIVE INTERACTION

In spite of the improvements in fitting the experimental data observed with the modifications of separate target and projectile density terms with different weights there are still discrepancies between the folded optical potentials and the "model independent" FB-potentials (Table 2). In particular the smaller radii of the former cannot be enlarged by any modification of the density dependence [20]. This is due to the fact that the integral quantities of the potentials are dominated by the low-density contribution from large nuclear radii.

Therefore, it was studied whether slight modifications of the radial part $t(r_{NN})$ of the effective interaction can lead to better agreement of the folded potentials with the model independent ones and to better representation of the experimental data. For that purpose the range parameter $a_1 = 4.0$ fm^{-1} of the repulsive part of $t(r_{NN})$ was kept fixed as before and the range parameter a_2 was adjusted in such a way that the "correct" potential radius $<r_v^2>^{1/2} = 4.345$ fm (see Table 2) was obtained for ^{40}Ca at $E_\alpha = 104$ MeV. The strength parameters V_1, V_2 were fitted together with the density dependent parameter γ using the $\rho^{2/3}$-dependence. The overall normalisation was set to $\lambda_R = 1$. The fits were made for different weight parameters w. The resulting parameter values are shown in Fig. 7.

The experimental data are equally well represented in the interval $0.6 < w < 1.0$ of the weight parameter w whereas a steep increase of χ^2/F is observed for $w < 0.5$. For values of $w < 0.4$ the solutions became extremely ambiguous. The parameters γ and w of the density dependent term $g(\rho)$ are linearly correlated within the broad minimum of χ^2/F, as expected, and non-linearly outside. The parameters V_1, V_2 and a_2 of $t(r_{NN})$, however, show very little variation around $w = 0.8$ and vary dramatically for $w < 0.6$.

This means that the density independent part $t(r_{NN})$ is nearly decoupled from the density dependent part $g(\rho)$ for $w \approx 0.8$. In other words, the ad hoc assumption [26] that these terms can be factorised is now empirically found to be valid under the modifications of $g(\rho)$ made in this analysis. This is also confirmed by the fact that the same weight parameter $w \approx 0.8$ is obtained as in the cases using the M3Y-interaction which means that the characteristic dependence of the effective interaction on the *densities* does not depend on the chosen *radial part* $t(r_{NN})$.

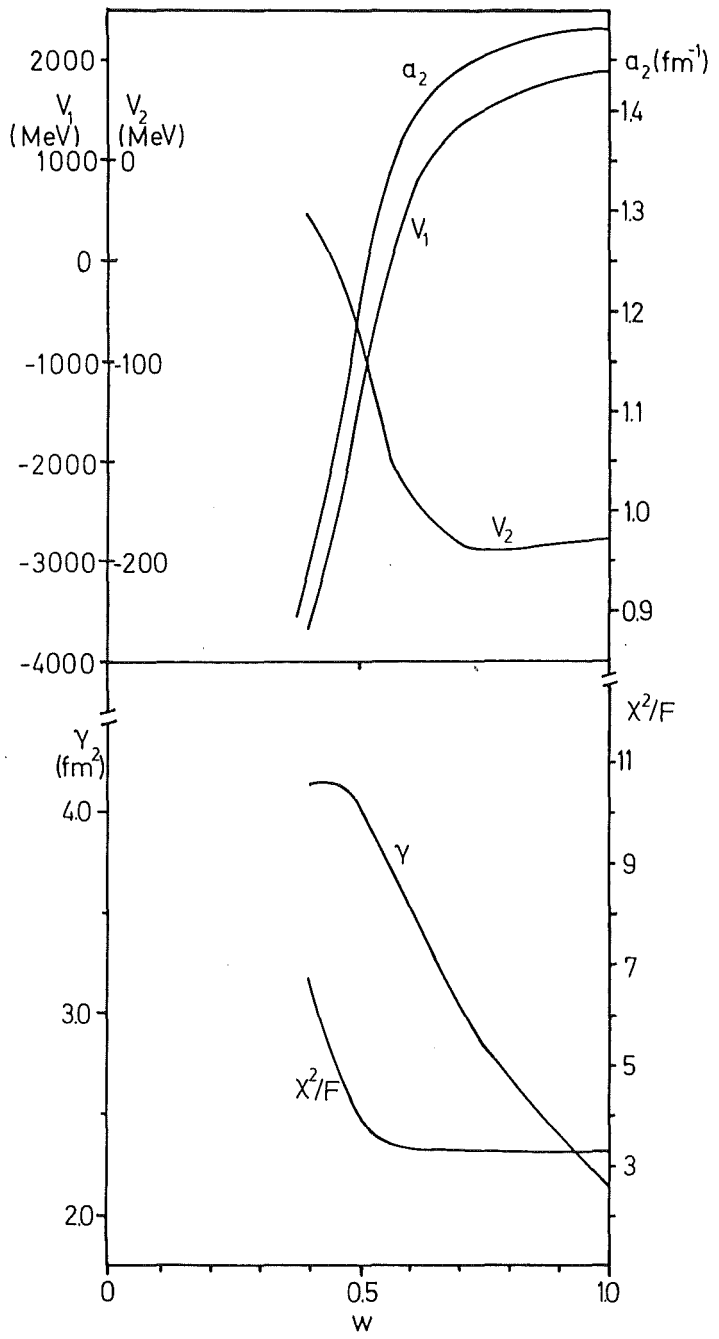

Fig. 7 Parameter values of the phenomenologically adjusted effective interaction versus the weight parameter w and corresponding values of $\chi^{2/F}$

The parameter values of the phenomenological effective interaction (PDDI) obtained for w = 0.8 are

V_1 = 1650 ± 81 MeV
a_1 = 4.0 fm^{-1} (fixed)
V_2 = -195.3 ±2.3 MeV
a_2 = 1.467 fm^{-1} (adjusted to reproduce $<r_V^2>^{1/2}$)

γ = 2.688 ± 0.043 fm^2

The corresponding calculated cross sections are displayed in Fig. 2 (lower part).

The radial part $t(r_{NN})$ of the PDDI-interaction is shown in Fig. 8 (dashed line) together with the M3Y-interaction (solid). The reduced strength of the phenomenological interaction at radii $0.5 < r < 2$ fm and the slightly larger tail for $r > 2$ fm lead to corresponding changes in the folded potential which is shown in Fig. 3 (solid line). The good agreement of this potential with the "model independent" FB- form is emphasized which is also documented by the characteristic integral quantities quoted in Table 6.

The results for the other target nuclei and energies obtained with the PDDI-interaction also quoted in Table 6 confirm the general relevance and validity of the modification of V_{NN} (eq. 2).

The value of the mean-square (ms) radius of $t(r_{NN})$ obtained in the described direct double-folding model analyses of elastic alpha-particle scattering is also noteworthy. From the given parameters a ms-radius $<r^2>_V^{eff}$ = 4.51 ± 0.15 fm^2 is calculated which is in excellent agreement with the value $<r^2>_V^{eff}$ = 5.3 ± 0.9 fm^2 derived from implicit folding interpretations of elastic nucleon scattering [17] assuming a cubic density dependence.

Returning to the shape of $t(r_{NN})$ (Fig. 8) one should note that the repulsive core of the effective NN-interaction is not essential for the elastic scattering of alpha-particles studied here, since these data are not sensitive to the short range part of the interaction. Equivalent fits to the experimental data and equivalent folded potentials were also obtained using a Gaussian plus Yukawa form with both parts attractive as shown in Fig. 8 (dotted line).

Table 6a: Double-folding potentials using the PDDI-interaction (see text).

E_α (MeV)	Target	λ_R	Y (fm^2)	$-J_v/4A$ (MeV fm^3)	$\langle r_v^2\rangle^{1/2}$ (fm)	$-J_w/4A$ (MeV fm^3)	$\langle r_w^2\rangle^{1/2}$ (fm)	χ^2/F
104	^{40}Ca	1.002(11)	2.695(22)	321.0	4.345	100.0	4.939	3.32
	^{50}Ti	1.028(10)	2.754(17)	308.9	4.501	92.8	5.067	2.03
	^{52}Cr	0.897(10)	2.465(23)	300.4	4.475	95.8	5.096	1.59
140	^{40}Ca	1.088(15)	2.920(25)	313.0	4.400	100.1	4.915	3.50
	^{50}Ti	1.107(11)	2.951(19)	300.3	4.550	94.4	5.118	3.06

Table 6b: Same as 6a, but with the parameter $\gamma = 2.688$ fm^2 ($E_\alpha = 104$ MeV) and $\gamma = 2.920$ fm^2 ($E_\alpha = 140$ MeV) fixed

E_α (MeV)	Target	λ_R	$-J_v/4A$ (MeV fm^3)	$\langle r_v^2 \rangle^{1/2}$ (fm)	$-J_w/4A$ (MeV fm^3)	$\langle r_w^2 \rangle^{1/2}$ (fm)	χ^2/F
104	^{40}Ca	1.002(2)	321.2	4.347	100.0	4.937	3.28
	^{50}Ti	0.999(2)	307.4	4.488	92.4	5.056	2.08
	^{52}Cr	1.002(2)	306.2	4.518	98.2	5.143	2.82
140	^{40}Ca	1.092(2)	314.1	4.400	101.3	4.914	4.23
	^{50}Ti	1.093(4)	300.4	4.543	94.6	5.106	3.22

Table 7: Double-folding optical potentials for $^{40}Ca(\alpha,\alpha)$ at $E_\alpha = 104$ MeV using the PDDI effective interaction and various parametrisations for the density dependence (w = 0.8, see text)

Model	λ_R	β' (fm^3)	γ	$-J_v/4A$ (MeV fm^3)	$\langle r_v^2 \rangle^{1/2}$ (fm)	$-J_w/4A$ (MeV fm^3)	$\langle r_w^2 \rangle^{1/2}$ (fm)	χ^2/F
DD exp	0.555(10)	11.58(29)	-	317.4	4.328	98.7	4.955	3.93
DD2/3	1.002(11)	-	2.695(22)*	321.0	4.345	100.0	4.939	3.32
DD3	0.872(9)	-	156.7(1.7)**	320.5	4.345	100.8	4.925	3.97

* fm^2 ** fm^9

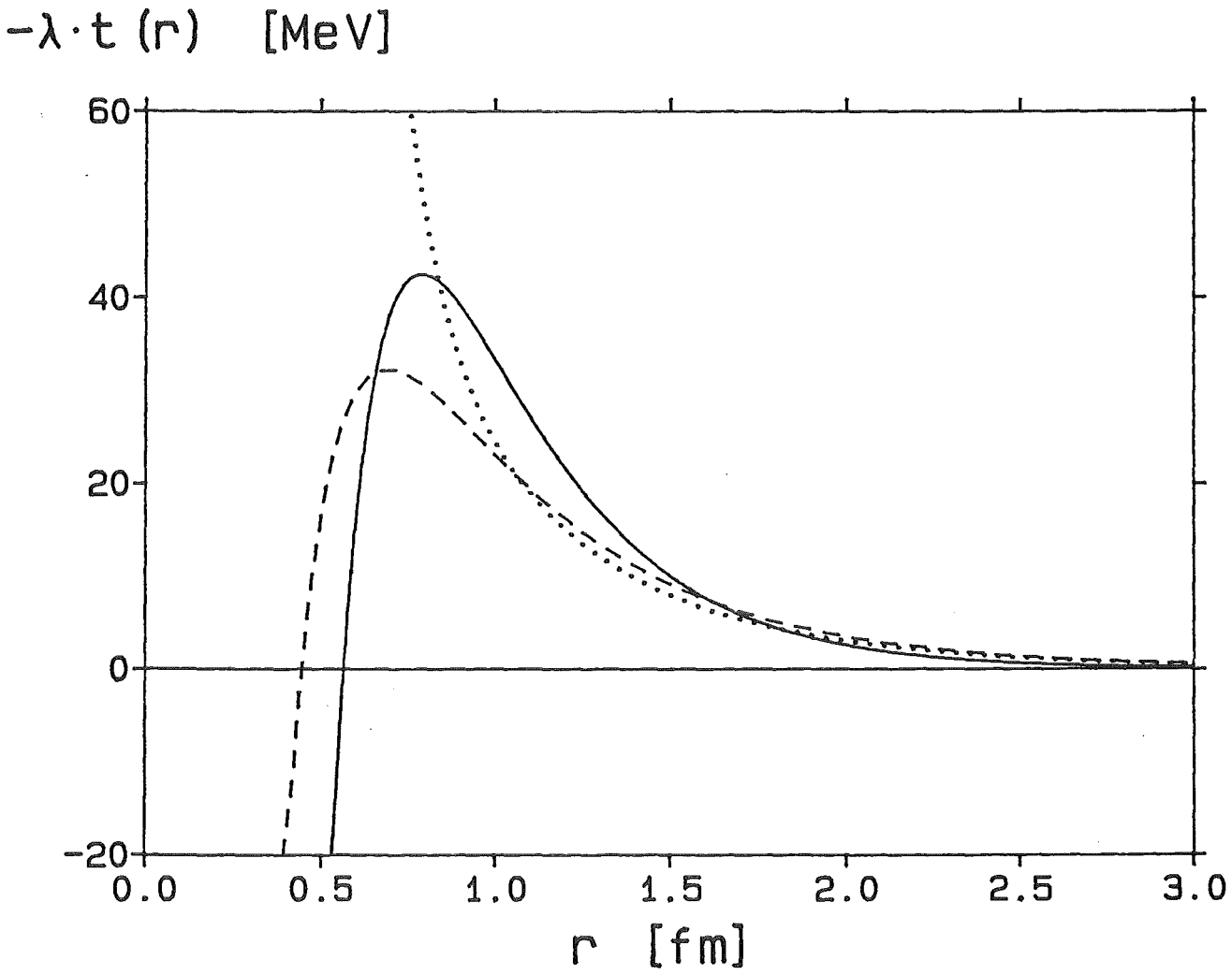

Fig. 8 Radial part t(r) of effective NN-interactions (see text)
Solid: M3Y
Dashed: PDDI (2Y)
Dotted: PDDI (G + Y)

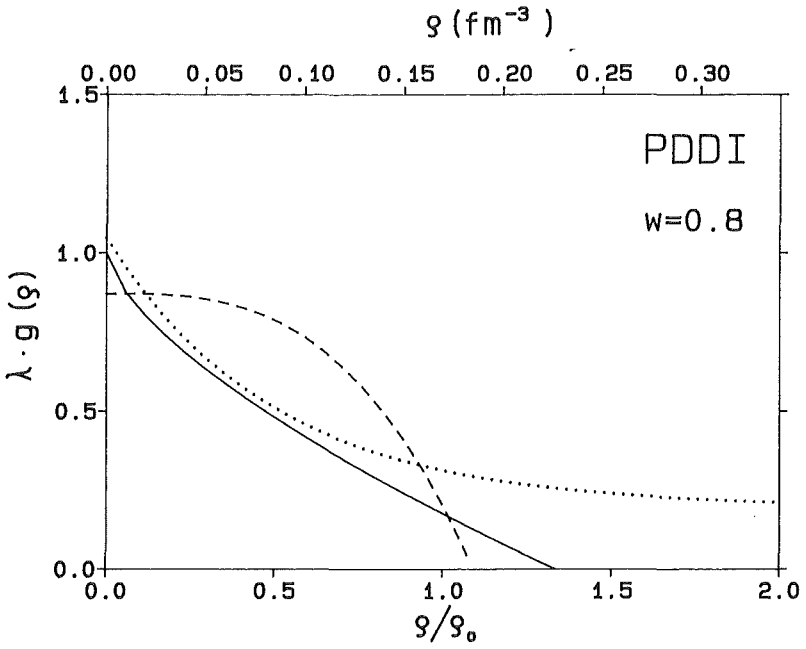

Fig. 9 Density dependence of the phenomenological interaction (PDDI, see text)
Solid: DD 2/3
Dashed: DD3
Dotted: DDexp

For completeness, the density dependence of V_{NN} is shown in Fig. 9 for the various parametrisations, which lead to equally good results as the chosen $\rho^{2/3}$-dependence. The corresponding parameter values are given in Table 7.

3.5. STUDIES OF NUCLEAR DENSITY DISTRIBUTIONS

The nuclear densities distributions entering into the folding integral (1) have so far been adopted from other sources. One may, however, also desire to use folding models for studies of isotopic or isotonic effects in nuclear density distributions. The refractive elastic scattering of alpha-particles is one of the strongly favoured [11,23,33] tools for this purpose thanks to its good radial sensitivity [23] (see Fig. 2). In fact, the advanced methods for the evaluation of nuclear scattering data [34] including "model independent" prescriptions either for the phenomenological optical potentials [21] or for the nuclear density distributions in folding models [6,35] were developed using the same data analysed in this work.

In these studies [11,23,35] the density dependent *single*-folding model was used where the density and size of the projectile is implicitly included in the radial shape of the effective interaction. Besides more practical aspects such as shorter computer time one of the main reasons for preferring the single-folding model were the open questions of density compression and gradient effects in double-folding models studied in this paper. Moreover, in rather fundamental work [8,36] it was shown that the single-folding model is indeed an adequate description for elastic alpha-particle scattering because intermediate excitation and polarisation of the projectile is negligible.

Nevertheless, it seems worthwhile after the present findings and modifications of the effective NN-interaction to compare single- and double-folding model analyses for studies of nuclear density distributions.

For this purpose we replace the adopted calculated nuclear densities [30,31] by phenomenological forms. In the first step, which aims at the study of the general behaviour depending on the chosen parametrisation of the density dependence, the two-parameter Fermi form (F2) is used

$$\rho_T(r) = \rho_o \left\{ 1 + exp \left[\left(r - c_m \cdot A^{1/3} \right) / a_m \right] \right\}^{-1} \qquad (9)$$

with c_m the half-way radius and a_m the diffuseness parameter. The normalisation of the density distribution to the target mass number A is provided by the factor ρ_o.

A less model dependent parametrisation for the nuclear density than through F2 is given by the flexible Fourier-Bessel form [6,11] (FB) which is here for the first time used in connection with double-folding models:

$$\rho_T(r) = \rho_{om}(r) + \sum_{\nu=1}^{N'} \beta_\nu \, j_o\left(\frac{\nu \pi r}{R'_c} \right). \qquad (10)$$

Here, $\rho_{om}(r)$ is a first approximation to the nuclear density, usually the best-fit F2-form, which is modified by the FB-series the volume integral of which is constraint to zero. The parameters β_ν of the "model independent" FB-densities were determined in fits to the experimental data in the second step of the analyses. For comparison, results of such FB-folding analyses using the density dependent *single*-folding model taken from Ref. 11) are quoted in Table 8.

Starting with the conventional DD M3Y-interaction [4] (see Sect. 3.1.) and varying the density parameters c_m and a_m in addition to λ_R led, as expected, to better fits to the experimental data than with fixed densities (see Table 3 and Table 9). The rms radii of the nuclear matter distributions and in particular their isotopic differences did not contradict other experimental results [33].

Slightly better fits but similar results concerning the densities were obtained with the radial part $t(r_{NN})$ of the M3Y-form combined with the weighted ($w = 0.8$) $\rho^{2/3}$ density dependence (eq. 5) as shown in Table 10. For these calculations the energy dependent parameter γ was taken from the ^{40}Ca "benchmark" results given in Table 5. However, as in the former case also in this case the folded real potentials deviated considerably from the "model independent" ones (see Table 2).

Replacing in these two models the Fermi distribution by the flexible Fourier-Bessel form [6,11] led to rather unstable results with unphysical oscillations in the densities. This observation is typical for cases where the folded potentials are unable to reproduce the best phenomenological potentials [11,23].

Table 8: Optical potentials and nuclear matter radii $<r_m^2>^{1/2}$ from *single*-folding model analyses using "model-independent" FB-densities (E_a = 104 MeV)
From Ref. [11].

Target	$<r_m^2>^{1/2}$ (fm)	$-J_v/4A$ (MeV fm^3)	$<r_v^2>^{1/2}$ (fm)	$-J_w/4A$ (MeV fm^3)	$<r_w^2>^{1/2}$ (fm)	χ^2/F
^{40}Ca	(3.38 ± 0.02)	320.5	4.350	102.3	4.908	2.1
^{50}Ti	3.55 ± 0.02	312.0	4.501	96.3	5.044	1.7
^{52}Cr	3.54 ± 0.02	302.2	4.480	97.3	5.073	1.4

Table 9: Nuclear matter densities (2-parameter Fermi distributions) and optical potentials obtained with the DD M3Y-interaction [4].

E_a (MeV)	Target	λ_R	c_m (fm)	a_m (fm)	$<r_m^2>^{1/2}$ (fm)	$-J_v/4A$ (MeV fm^3)	$<r_v^2>^{1/2}$ (fm)	$-J_w/4A$ (MeV fm^3)	$<r_w^2>^{1/2}$ (fm)	χ^{2}/F
104	^{40}Ca	1.258(2)	1.116(11)	0.427(13)	3.356(34)	305.5	4.227	98.5	4.984	5.8
	^{50}Ti	1.243(2)	1.169(7)	0.348(11)	3.578(24)	296.7	4.385	92.6	5.070	2.1
	^{52}Cr	1.239(3)	1.115(8)	0.393(10)	3.539(26)	289.9	4.375	95.2	5.132	3.0
140	^{40}Ca	1.303(5)	1.212(16)	0.322(24)	3.427(50)	295.9	4.258	102.4	4.926	5.8
	^{50}Ti	1.295(6)	1.163(15)	0.375(19)	3.600(48)	287.3	4.427	92.8	5.158	6.2

When, however, the phenomenological effective interaction (PDDI) was used the fit to the experimental data was considerably improved and the folded optical potentials agreed with the FB-potentials. This is shown in Table 11a where fixed density dependence parameters γ had been taken from Table 5. Due to the correlation of the parameters λ_R and γ one may also keep the normalisation λ_R fixed and optimise γ in order to fit the experimental data. The minor influence of such choices on the resulting parameters and integral moments of the nuclear matter densities is demonstrated in Tables 11b and c, where the parameter λ_A is calculated from Table 2 by the relationship.

$$\lambda_A(A) = \left| J_v/4A\,(A) \right| / \left| J_v/4A\,(^{40}Ca) \right| \qquad (11)$$

Similar studies using the *single*-folding model led to corresponding results [23].

Adopting the results from Table 11c as first approximation $\rho_{om}(r)$ (see eq. 10) FB-densities were introduced into the analyses of the 104 MeV data the angular accuracy of which is sufficient for such flexible forms. In contrast to the case using the M3Y-interaction very stable conditions were found with the FB-densities. Figure 10 shows, as an example, the nuclear density obtained for ^{40}Ca which reproces the calculated density [30] used to derive the PDDI-interaction. This self-consistent result is another confirmation for the validity of the model.

The difference between the nuclear densities of ^{40}Ca and ^{52}Cr as determined from the double-folding model analyses [11] using "model independent" FB-densities are shown in Fig. 11. The error band includes also uncertainties in the effective interaction (PDDI) [23]. The corresponding nuclear matter rms-radii and integral quantities of the optical potentials are compiled in Table 12. The good overall consistency with the FB-potentials (Table 2) as well as with the corresponding *single*-folding model analyses (Table 8) is emphasized. However, one should keep in mind that such a consistent picture could only be drawn when infering phenomenological approaches into the double-folding model which are of the same quality as those in the single-folding model [23]. Therefore, it is questionable whether the expenditure of double-folding is necessary for such analyses since the contribution from the projectile density is anyway canceled out in density *differences*.

Table 10: Nuclear matter densities (F2) and optical potentials obtained with the M3Y-interaction and weighted (w = 0.8) $\rho^{2/3}$ density dependence (DD 2/3, see text); $\gamma = 2.267$ fm^2 ($E_\alpha = 104$ MeV), $\gamma = 2.528$ fm^2 ($E_\alpha = 140$ MeV)

E_α (MeV)	Target	λ_R	c_m (fm)	a_m (fm)	$\langle r_m^2 \rangle^{1/2}$ (fm)	$-J_v/4A$ (MeV fm^3)	$\langle r_v^2 \rangle^{1/2}$ (fm)	$-J_w/4A$ (MeV fm^3)	$\langle r_w^2 \rangle^{1/2}$ (fm)	χ^2/F
104	^{40}Ca	1.481(6)	1.055(15)	0.506(12)	3.369(41)	308.8	4.254	99.1	4.966	5.0
	^{50}Ti	1.451(4)	1.119(9)	0.439(9)	3.586(27)	299.0	4.406	'93.0	5.069	2.0
	^{52}Cr	1.484(6)	1.049(8)	0.482(8)	3.523(25)	292.3	4.398	96.2	5.107	2.5
140	^{40}Ca	1.575(11)	1.185(18)	0.385(18)	3.450(52)	300.3	4.288	105.1	4.891	3.1
	^{50}Ti	1.620(13)	1.105(18)	0.448(17)	3.566(54)	290.1	4.452	94.8	5.131	4.6

Table 11a: Same as Table 10, but PDDI-interaction
$\gamma = 2.688$ fm^2 ($E_\alpha = 104$ MeV), $\gamma = 2.920$ fm^2 ($E_\alpha = 140$ MeV).

E_α (MeV)	Target	λ_R	c_m (fm)	a_m (fm)	$\langle r_m^2 \rangle^{1/2}$ (fm)	$-J_v/4A$ (MeV fm^3)	$\langle r_v^2 \rangle^{1/2}$ (fm)	$-J_w/4A$ (MeV fm^3)	$\langle r_w^2 \rangle^{1/2}$ (fm)	χ^2/F
104	^{40}Ca	0.987(8)	1.098(16)	0.471(11)	3.395(42)	321.2	4.340	100.5	4.929	3.3
	^{50}Ti	0.963(5)	1.156(9)	0.405(8)	3.626(26)	309.3	4.497	93.6	5.058	2.0
	^{52}Cr	1.028(10)	1.049(15)	0.470(12)	3.500(44)	301.2	4.487	95.4	5.095	1.8
140	^{40}Ca	1.008(8)	1.241(17)	0.350(18)	3.536(49)	316.7	4.390	106.3	4.875	1.3
	^{50}Ti	1.029(9)	1.176(11)	0.389(9)	3.654(32)	300.6	4.547	96.3	5.102	2.6

Table 11b: Same as Table 11a, but $\lambda_R = 1$ and parameter γ varied

E_α (MeV)	Target	γ (fm^2)	c_m (fm)	a_m (fm)	$<r_m^2>^{1/2}$ (fm)	$-J_v/4A$ (MeV fm^3)	$<r_v^2>^{1/2}$ (fm)	$-J_w/4A$ (MeV fm^3)	$<r_w^2>^{1/2}$ (fm)	χ^2/F
104	^{40}Ca	2.701(13)	1.080(13)	0.483(11)	3.378(36)	320.7	4.343	100.1	4.932	3.4
	^{50}Ti	2.752(8)	1.139(7)	0.416(8)	3.599(22)	309.5	4.499	93.8	5.060	1.9
	^{52}Cr	2.659(12)	1.068(12)	0.458(11)	3.526(36)	301.6	4.484	96.0	5.090	1.7
140	^{40}Ca	3.097(15)	1.229(14)	0.347(14)	3.502(39)	315.3	4.389	105.7	4.879	1.2
	^{50}Ti	2.999(19)	1.151(15)	0.406(14)	3.615(45)	301.1	4.550	95.7	5.102	3.2

Table 11c: Same as Table 11a, but $\lambda_R = (1+\lambda_A)/2$ (see text) and parameter γ varied

E_0 (MeV)	Target	γ (fm^2)	c_m (fm)	a_m (fm)	$<r_m^2>^{1/2}$ (fm)	$-J_v/4A$ (MeV fm^3)	$<r_v^2>^{1/2}$ (fm)	$-J_w/4A$ (MeV fm^3)	$<r_w^2>^{1/2}$ (fm)	χ^2/F
104	^{40}Ca	2.701(13)	1.080(13)	0.483(11)	3.378(36)	320.7	4.343	100.1	4.932	3.4
	^{50}Ti	2.695(9)	1.152(9)	0.409(9)	3.622(27)	309.4	4.498	94.1	5.062	2.2
	^{52}Cr	2.594(9)	1.072(10)	0.461(9)	3.542(30)	300.7	4.481	95.6	5.094	1.6
140	^{40}Ca	3.097(15)	1.229(14)	0.347(14)	3.502(39)	315.3	4.389	105.7	4.879	1.2
	^{50}Ti	2.971(13)	1.169(12)	0.391(12)	3.639(36)	301.0	4.548	96.6	5.097	2.6

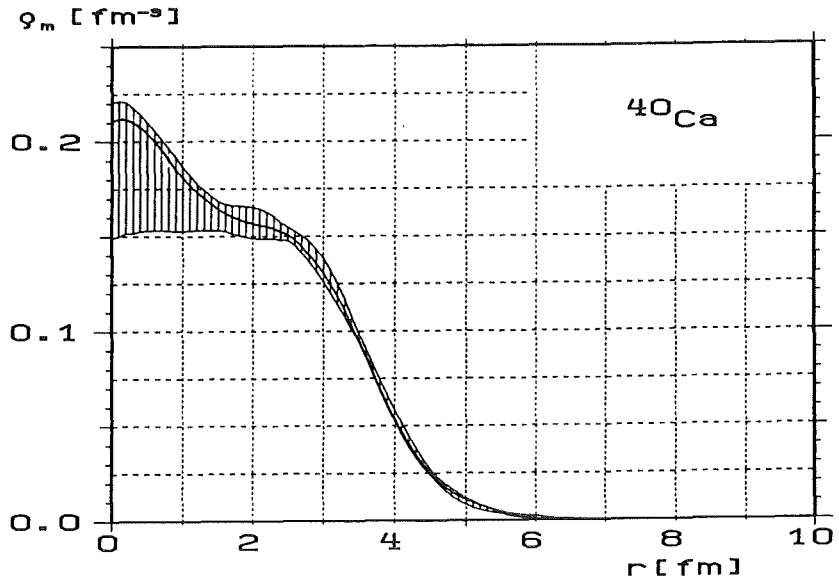

Fig. 10 Nuclear matter density distribution of ^{40}Ca
Solid: calculated density [30]
Hatched: best-fit FB-density

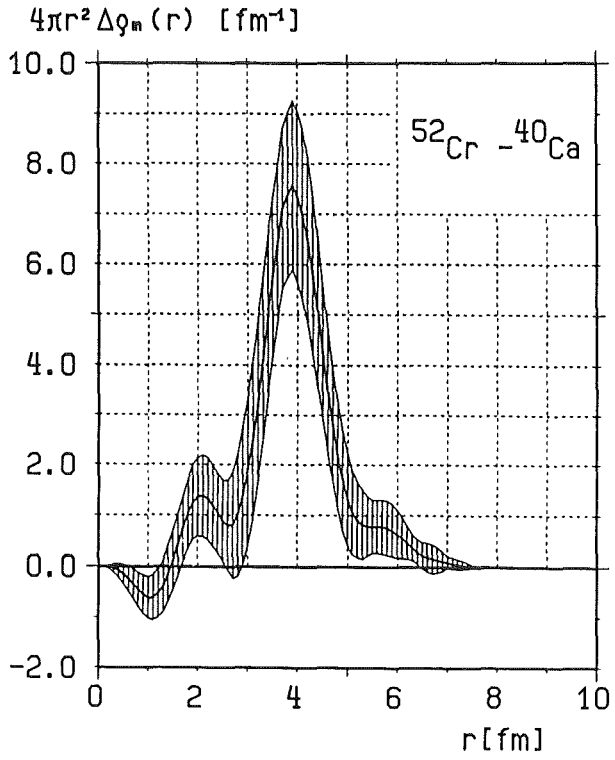

Fig. 11 Difference between the nuclear matter densities of ^{52}Cr and ^{40}Ca as obtained from double-folding model analyses of elastic alpha-particle scattering

Table 12: Optical potentials and nuclear matter rms-radii from double-folding model analyses with PDDI-interaction and FB-densities

Target	$<r_m^2>^{1/2}$ (fm)	$-J_v/4A$ (MeV fm^3)	$<r_v^2>^{1/2}$ (fm)	$-J_w/4A$ (MeV fm^3)	$<r_w^2>^{1/2}$ (fm)	χ^2/F
^{40}Ca	3.368 ± 0.026	320.6	4.342	99.9	4.931	3.2
^{52}Cr	3.536 ± 0.028	299.9	4.470	95.5	5.095	1.7

4. Summary and conclusions

The density dependence of effective NN-interactions was studied in double-folding model analyses of elastic alpha-particle scattering. Different semi-phenomenological parametrisations often used in the past were compared. As an essential modification separate target and projectile density terms with different weights were introduced. With this modification the various forms of density dependence were found to be equivalent in fitting the experimental data. This means in particular that the recently suggested [17-19] cubic density dependence of an effective NN-interaction is successful in describing very accurate elastic scattering cross sections. However, the experimental data are not able to distinguish this form from others as e.g. a $\rho^{2/3}$ dependence. Therefore, conclusions about the correct density dependence of two-body effective interactions for densities much larger than those of normal nuclear matter ($\rho_0 \approx 0.17$ fm^{-3}), which was subject of recent discussions [17], can not be drawn from the present analyses.

Full consistency of the folded optical potentials with the best-fit "model independent" potentials could be achieved when the radial part of the effective interaction was slightly adjusted. The ms radius and density dependence of the effective interaction obtained in this way was found to be in excellent agreement with other studies [17].

Concluding on the possibility of extracting information on nuclear density distributions from elastic alpha-particle scattering it was shown that it is not predominantly a question of using a *single* or *double*-folding model. Rather it is the question of starting from first principles or of ending up with results consistent with the best phenomenological potentials. In other words, the philosophy behind the different methods and the measure of validity are the important points distinguishing between alternative approaches and it is a matter of *taste*, which way to follow. In a more fundamental philosophy one has to include all important effects from first principles and, if possible, without adjustable parameters [15]. However, even in the best approaches at least one parameter had to be optimised and considerable deficiencies in fitting the experimental data still remain. It must be noted, that the iterative procedure for calculating the finite range exchange term is rather tedious and less suitable for extensive studies of nuclear densities using "model independent" forms.

In the other philosophy, which was followed in this study, the consistency between the folding model and phenomenological "model independent" potentials and the representation of measured cross sections are the dominant measures of its validity. In order to fulfill the well-defined requirements several phenomenological approaches must be introduced. At this level, single [23] and double-folding models are equivalent and well suited for studies of isotonic and isotopic *differences* of nuclear density distributions, since both models inevitably need "bendmark" nuclei for calibration of the effective interaction.

Acknowledgements: The author would like to thank Profs. Drs. E. Friedman, H. Rebel, B. Sinha and D.K. Srivastava for fruitful and stimulating discussions. The help of Mr. J. Oehlschläger with computer software is gratefully acknowledged.

References

1) G.R. Satchler and W.G. Love, Phys. Rep. **55** (1979) 183
2) G. Bertsch, J. Borysowicz, H. McManus and W.G. Love, Nucl.Phys. **A 284** (1977) 399
3) G.R. Satchler, Nucl. Phys. **A 329** (1979) 233
4) A.M. Kobos, B.A. Brown, P.E. Hodgson, G.R. Satchler and A. Budzanowski, Nucl. Phys. **A 384** (1982) 65
5) A.K. Chaudhuri, Nucl. Phys. **A 449** (1986) 243
6) E. Friedman, H.J. Gils, H. Rebel and Z. Majka, Phys. Rev.Lett. 41 (1978) 1220
7) Z. Majka, H.J. Gils and H. Rebel, Z. Phys. **A 288** (1978) 139
8) F. Duggan, M. Lassaut, F. Michel and N. Vinh Mau, Nucl. Phys. **A 355** (1981) 141
9) H.J. Gils, E. Friedmann, H. Rebel, J. Buschmann, S. Zagromski, H. Klewe-Nebenius,B. Neumann, R. Pesl and G. Bechtold, Phys. Rev. **C 21** (1980) 1239
10) E. Friedman, H.J. Gils, H. Rebel and R. Pesl, Nucl. Phys. **A 363** (1981) 137
11) H.J. Gils, H. Rebel and E. Friedman, Phys. Rev. **C 29** (1984) 1295
12) A.M. Kobos, B.A. Brown, R. Lindsay and G.R. Satchler, Nucl. Phys. **A 425** (1984) 205
13) J.P. Jeukenne, A. Lejeune and C. Mahaux, Phys. Rev. **C 16** (1977) 80
14) J.-P. Jeukenne and C. Mahaux, Z. Phys. **A 302** (1981) 233
15) A.K. Chaudhuri, D.N. Basu and B. Sinha, Nucl. Phys. **A 439** (1985) 41
16) H. Abele, H.J. Hauser, A. Körber, W. Leitner, R. Neu, H. Plappert, T. Rohwer, G. Staudt, M. Straßer, S. Welte, M. Walz, P.D. Eversheim and F. Hinterberger, Z. Phys. **A 326** (1987) 373
17) W.J. Thompson, T.L. McAbee and R.L. Varner, Phys. Lett. **182 B** (1986) 247
18) G.E. Brown et al., Commun. Nucl. Part. Phys., to be published
19) R. Schiavilla, V.R. Pandharipande and R.B. Wiringa,Nucl. Phys. **A 449** (1986) 219
20) H.J. Gils, Z. Phys. **A 317** (1984) 65
21) E. Friedman and C.J. Batty, Phys. Rev. **C 17** (1978) 34
22) H.J. Gils, E. Friedman, H. Rebel, J. Buschmann, S. Zagromski,H. Klewe-Nebenius, B. Neumann, R. Pesl and G. Bechtold, KfK-Report 2838, Kernforschungszentrum Karlsruhe (1979)
23) H.J. Gils, KfK Report 3765, Kernforschungszentrum Karlsruhe (1984)
24) D.A. Goldberg, S.M. Smith and G.F. Burdzik, Phys. Rev. **C 10** (1974) 1362

25) P.L. Roberson, D.A. Goldberg, N.S. Wall, L.W. Woo and H.L. Chen, Phys. Rev. Lett. 42 (1979) 54
26) F. Petrovich, D. Stanley and J.J. Bevelacqua, Phys. Lett.71B (1977) 259
27) W.D. Myers, "Droplet Model of Atomic Nuclei", IFL-Plenum, New-York (1977)
28) H. Leeb, H. Fiedeldey and R. Lipperheide, Phys. Rev. C 32 (1985) 1223
29) H.J. Gils, H. Rebel and E. Friedman, KfK-Report 3556, KernforschungszentrumKarlsruhe (1983)
30) B.A. Brown, S.E. Massen and P.E. Hodgson, J. Phys. G 5 (1979) 1655
31) P.-G. Reinhardt and J. Friedrich, private communication
32) D.K. Srivastava, Phys. Lett. 113 B (1982) 353
33) C.J. Batty, E. Friedman, H.J. Gils and H. Rebel, in "Advances in Nuclear Physics" ed. J.W. Negele and E. Vogt, (Plenum Press, New York) (in press)
34) H.J. Krappe and R. Lipperheide (eds.) *Advanced Methods in the Evaluation of Nuclear Scattering Data*, Lecture Notes in Physics 236 (1985)
35) I. Brissaud and M.K. Brussel, J. Phys. G 3 (1977) 481
36) N. Vinh Mau, Phys. Lett. 71 B (1977) 5